Efficient Hybrid White Organic Light-Emitting Devices with a Reduced Efficiency Roll-off Based on a Blue Fluorescent Emitter of Which Charge Carriers Are Ambipolar and Electric-Fie...

ARTICLE *in* THE JOURNAL OF PHYSICAL CHEMISTRY C · DECEMBER 2010

Impact Factor: 4.77 · DOI: 10.1021/jp109921e

THE JOURNAL OF PHYSICAL CHEMISTRY C

ARTICLE

pubs.acs.org/JPCC

Efficient Hybrid White Organic Light-Emitting Devices with a Reduced Efficiency Roll-off Based on a Blue Fluorescent Emitter of Which Charge Carriers Are Ambipolar and Electric-Field Independent

Tianyu Zhang,[†] Mo Liu,[†] Tong Li,[†] Jian Ma,[†,‡] Dali Liu,[†] Wenfa Xie,[*,†] Cheng-Lung Wu,[§] Shun-Wei Liu,[§] Shih-Chieh Yeh,[§] and Chin-Ti Chen[*,§]

[†]State Key Laboratory on Integrated Optoelectronics, College of Electronic Science and Engineering, Jilin University, Changchun, 130012, People's Republic of China

[‡]Department of Physics, Jilin University, Changchun 130023, People's Republic of China

[§]Institute of Chemistry, Academia Sinica, Taipei, 11529, Taiwan

ABSTRACT: Efficient hybrid white organic light-emitting devices (WOLEDs) were developed using an ambipolar blue fluorescent emitter 2-diphenylamino-7-(2,2′′-diphenylvinyl)-9,9′-spirobifluorene (DPV) which has a relatively electric-field independent hole and electron mobilities. The effects of the triplet energies and charge transporting properties of the blue materials on the performance of the device are discussed. By using such a blue emitter in the device, a broader charge recombination zone is formed, and the energy loss is reduced. WOLEDs with a maximum current efficiency of 25.1 cd/A which shift to 19.5 cd/A at 10000 cd/m^2 have been achieved. The power efficiency and the Commission Internationale de l'Eclairage coordinates of the device are 14.1 lm/W and (0.41, 0.41) at 1000 cd/m^2. By attaching a microlens array (MLA) on the backside of the substrate, the outcoupling of electroluminescence in the forward direction is enhanced, resulting in elevated power efficiency 18.6 lm/W at 1000 cd/m^2.

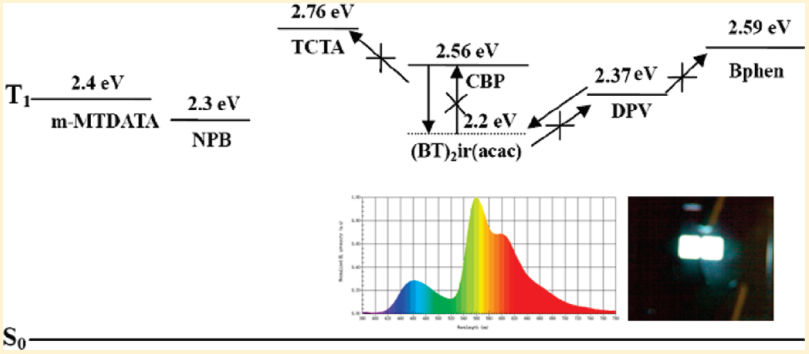

White organic light-emitting devices (WOLEDs) have been of considerable interest in recent years because of their potential applications as full color displays, backlights for liquid crystal displays, and solid-state lighting sources.[1−3] Various methods have been proposed to realize efficient WOLEDs.[4−16] Among these approaches, WOLEDs employing phosphorescent materials are most effective because phosphorescent materials can harvest both singlet and triplet excitons, which leads to the potential for achieving 100% internal quantum efficiency. However, blue phosphorescent devices exhibited a short operational lifetime that limits the stability of all-phosphor-doped WOLEDs.[12] Thus, the development of novel hybrid WOLEDs with the combination of blue-fluorescent (F) and green−red or yellow-phosphorescent (P) emitters may solve these problems and obtain efficient and stable WOLEDs. Recent conceptual advancement leads to many exciting F/P architectures, such as manipulating singlet and triplet excitons within an ambipolar host,[17] introducing multifunctional dopants,[18,19] and the utilization of a phosphorescent sensitizer or a p-i-n junction structure.[20,21] A high triplet energy fluorescent blue emitter is important in the F/P WOLEDs because it could harvest its triplet excitons by letting them diffuse to an orange phosphorescent iridium complex.[20] However, the main challenges of the hybrid WOLED include the reduction of the efficiency roll-off and the stability of the color coordinates.[22] In this paper, an efficient hybrid WOLED with a relatively high triplet energy blue fluorescent emitter is reported. We demonstrated that charge transporting property of the blue fluorescent emitter is also important for the F/P WOLED. An ambipolar blue fluorescent emitter with voltage-independent mobility could let us to design a WOLED with a broader charge recombination zone easily, and a efficient hybird WOLED with stable color coordinates and reduced efficiency roll-off can be achieved.

WOLEDs with the structure of ITO/4,4′,4′′-tris(3-methylphenylphenylamino)-triphenylamine (m-MTDATA: 20 nm)/*N*,*N*′-bis-(1-naphthyl)-*N*,*N*′-diphenyl-1,1-biphenyl-4,4′-diamine (NPB: 20 nm)/4,4′,4′′-tris(*N*-carbazolyl)-triphenylamine (TCTA: 10 nm)/CBP: 8%$(BT)_2$Ir(acac) (15 nm)/blue emitter (10 nm)/4,7-diphenyl-1,10-phenanthroline (Bphen: 30 nm)/LiF/Al are fabricated [CBP and $(BT)_2$Ir(acac) stands for 4,4′-*N*,*N*′-dicarbazole-biphenyl and iridium(III) bis(2-phenylbenzothiozolato-*N*,$C^{2'}$) acetylacetonate, respectively]. The devices with 2-diphenylamino-7-(2,2′′-diphenylvinyl)-9,9′-spirobifluorene (DPV)[23] or NPB as blue emitter were named as Device A and B, respectively. Except for DPV material, other

Received: October 15, 2010
Revised: December 9, 2010
Published: December 22, 2010

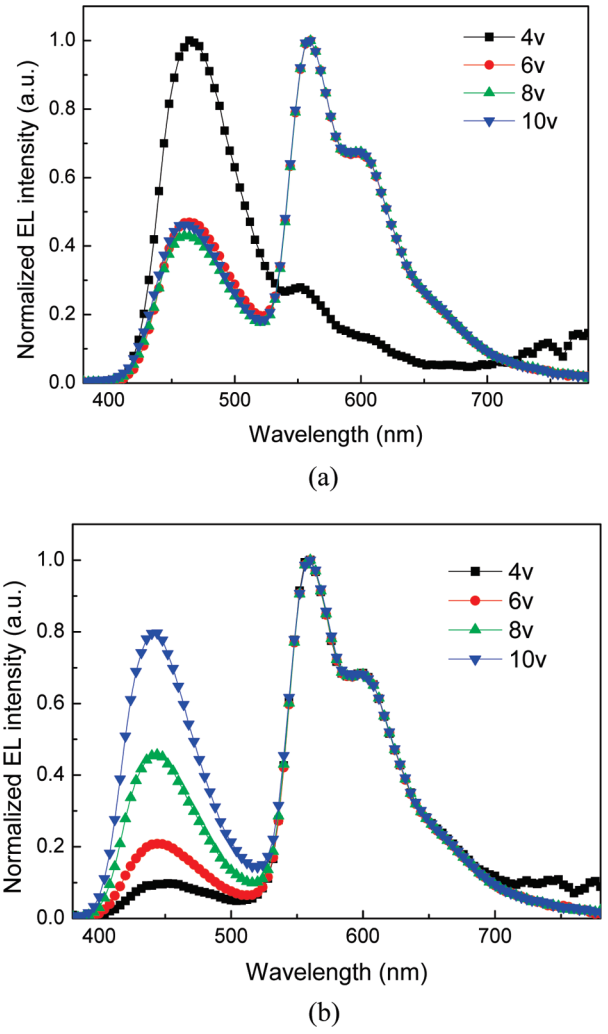

Figure 1. Normalized EL spectra of (a) Device A and (b) Device B.

organic materials used in this work were purchased from Luminescence Technology Corporation and used without further purification. Prior to the device fabrication, ITO-coated glass substrates were carefully cleaned by scrubbing and sonication. All organic layers were deposited onto the substrate in high vacuum (10^{-4} Pa) by thermal evaporation with a rate of 0.1−0.2 nm/s. Then, a bilayer cathode of LiF/Al was subsequently vapor-deposited onto the organic films. The layer thickness and the deposition rate of the materials were monitored in situ using an oscillating quartz thickness monitor. The electroluminescent (EL) spectra and 1931 Commission Internationale de l'Eclairage (CIE) coordinates of the devices were measured by using a PR650 spectroscan spectrometer. The luminance−voltage and current−voltage characteristics were measured simultaneously with a programmable Keithley 2400 voltage−current source. All measurements were carried out at room temperature under ambient conditions.

Figure 1 shows the normalized EL spectra of devices A and B at different applied voltages. The EL spectrum of the WOLEDs exhibit the peak wavelengths at 440, 464, and 560 nm, which originate from NPB, DPV, and $(BT)_2Ir(acac)$, respectively. It can be seen from Figure 1a that, at a low applied voltage (4 V), the emission spectra of Device A shows a little yellow emission from $(BT)_2Ir(acac)$. As the voltage changes from 6 to 10 V, the emission intensity of $(BT)_2Ir(acac)$ increases with a minor change in the intensity of the emission from DPV. In contrast, the emission spectra of the Device B shows a little blue emission at 4 V. As the voltage increasing, the emission intensity of NPB increases step by step. The color coordinates of Device A are only slightly shifted by (0.03, 0.02) from 6 to 10 V. However, that of the Devcie B shifts significantly by (0.07, 0.09).

To investigate the above phenomena, the energy level and triplet energy level diagram of the WOLED is shown in Figure 2. The triplet energy is derived from the high energy peak at 524 nm as measured by gated phosphorescence (200 ns of delayed time) of a DPV thin film at 10 K. The estimated triplet state energy is about 2.37 eV which is higher than that of NPB (2.3 eV),[24] and this is considerably higher than that of $(BT)_2ir(acac)$ (2.2 eV). From the triplet energy alignments, it can be speculated that there should be an excellent triplet energy confinement on the emissive layers in the WOLEDs. We know that the hole mobility μ_h and the electron mobility μ_e of NPB are both electric-filed dependent. Generally, the values of μ_h for NPB are between 3×10^{-4} and 6×10^{-4} $cm^2/(V\,s)$.[25] On the other hand, μ_e exhibits a negative field dependence when $F < 0.1$ MV/cm. In between a field strength of $0.1 < F < 0.25$ MV/cm, μ_e has values between 5×10^{-4} and 6×10^{-4} cm/(V s). It can be seen that at a low filed, $\mu_e > \mu_h$, as the filed increases, a decreased electron mobility is observed for NPB. In contrast, the charge carrier mobility of DPV is relatively electric-field independent; the value of μ_h for DPV is higher than its μ_e in a wide range of electric-field.[26]

Taking in account the carrier transport properties of blue emission and energy level of WOLEDs as described above, it can be assumed that the charge recombination zone of free electrons and holes is situated close to the DPV/Bphen interface in Device A at low voltage. Singlet excitons that are created in the DPV layer may either undergo a direct radiative decay or be transferred via Förster transfer to the CBP:$(BT)_2Ir(acac)$ layer. This transfer is a process leading to an increase in yellow emission. Since the triplet energy of DPV is higher than that of $(BT)_2Ir(acac)$ and triplet energy of Bphen (2.59 eV) is higher than that of DPV, the triplet excitons may diffuse toward the adjacent CBP:$(BT)_2Ir(acac)$ layer where they can again decay radiatively. Therefore, there is little phosphorescent yellow emission in Device A at low voltage, and the creation of triplet excitons on CBP: $(BT)_2Ir(acac)$ layer will start only above a certain voltage (≥4 V in our cases). As the applied voltage increases, the phosphorescent yellow emission increases because more triplet excitons are created in the CBP:$(BT)_2Ir(acac)$ layer. The charge recombination zone will formed both at DPV and CBP:$(BT)_2Ir(acac)$ layer because of the high electron and hole mobility of CBP and DPV. The lesser electric-field dependence on the hole and electron mobility of DPV and CBP layer led to a relative constant charge recombination zone in Device A, which will reduce the triplet−triplet annihilation (TTA)[27−29] and induce relative constant EL spectra and CIE coordinates of the device.

In Device B, in contrast, the recombination zone is situated at the TCTA/CBP:$(BT)_2Ir(acac)$ interface at low voltage. The creation of singlet excitons on NPB layer will also start only above a certain voltage (≥4 V in our cases). For a high applied voltage, the charge recombination zone of Device B shift to the NPB layer due to the carrier mobility of NPB is electric-field dependent. Synchronously, more excitons accumulated at the TCTA/CBP:$(BT)_2Ir(acac)$ interface induce significant TTA which reduce the emission efficiency of phosphors, and consequently, the fluorescent blue emission displays a steady increase.

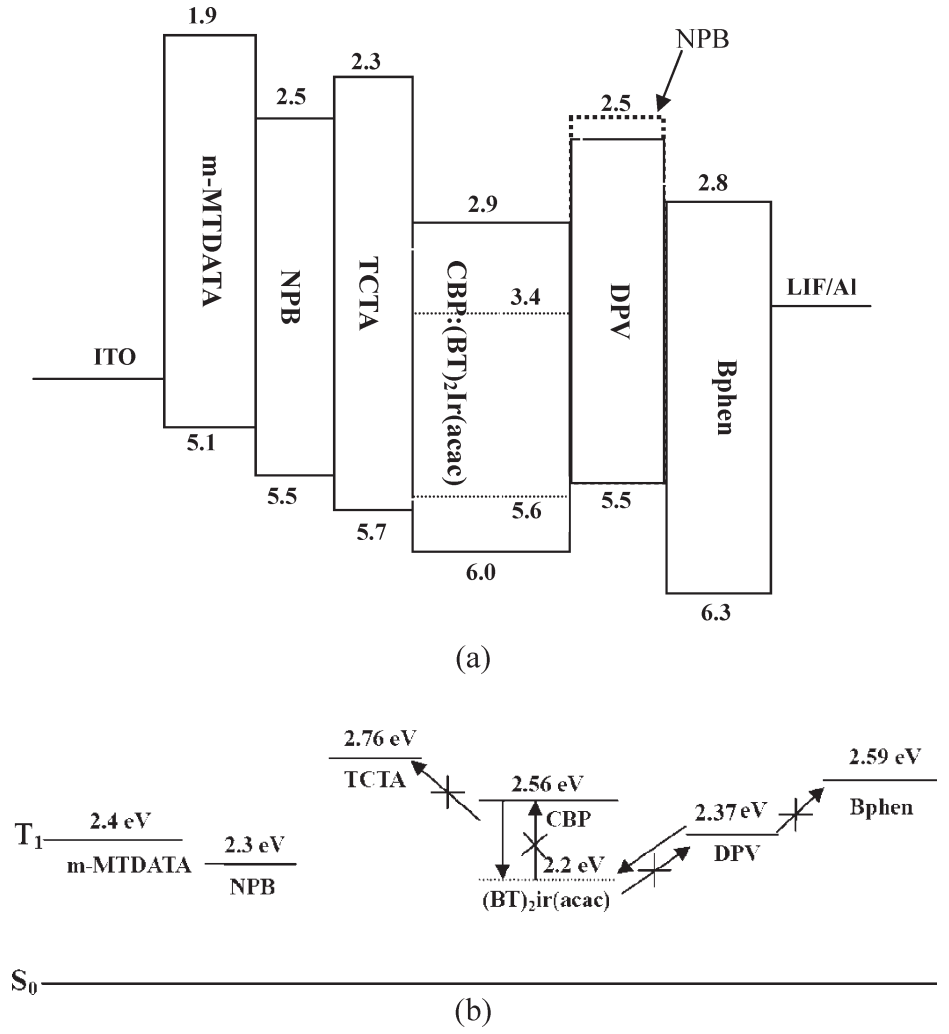

Figure 2. (a) Alignment of energy levels and (b) triplet state energy level diagram of WOLEDs.

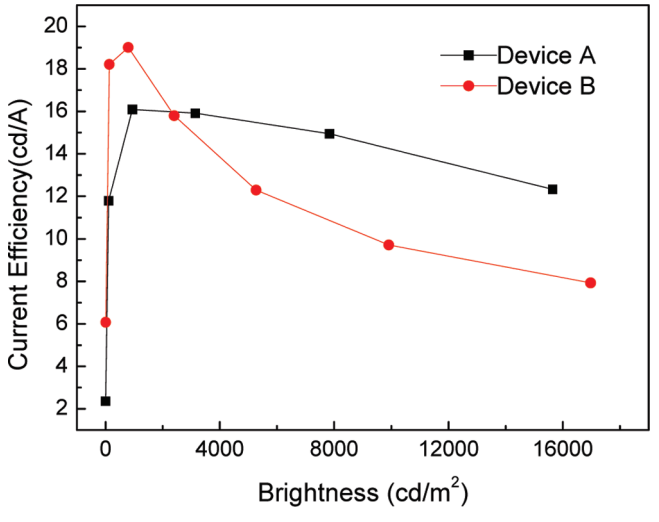

Figure 3. Current efficiency−luminance characteristics of Devices A and B.

Current efficiency−luminance characteristics of the WOLEDs are shown in Figure 3. The maximum current efficiency of Devices A and B are 16.1 and 19.0 cd/A, respectively. It can be seen that although the current efficiency of Device A is lower than that of Device B, the efficiency roll-off of the Device A is less than that of the Device B. From the brightness at maximum current efficiency to 10000 cd/m^2, the efficiency roll-off of the Devices A and B are 11.8% and 49.0%, respectively. On the basis of the above analysis, at a low applied voltage, most of the electroluminescence is from phosphorescent material $(BT)_2$ir(acac) in Device B but is from fluorescent material DPV in Device A. Thus, the maximum current efficiency of Device B is higher than that of Device A. However, the TTA in Device B is significant at high current density which induces the serious efficiency roll-off of the device. Therefore, using an ambipolar blue emitter with relatively electric-field-independent mobility, such as DPV, greatly benefits the reduction of efficiency roll-off and stability of color coordinates in fluorescent/phosphorescent hybrid WOLEDs.

Performances of this kind of WOLEDs can be further improved by adjusting the concentration of phosphorescent materials and the thickness of the yellow phosphorescent layer. More efficient WOLEDs are demonstrated by fixing the thickness of both light emitting layers at 25 nm, adjusting the thickness of CBP:$(BT)_2$ir(acac) from 10 to 14 nm, and increasing the concentration of phosphorescent materials to 10%. The structure of three WOLEDs are as follows: glass substrate/ITO/m-MTDATA (20 nm)/NPB (20 nm)/TCTA (10 nm)/CBP:10%

dx.doi.org/10.1021/jp109921e |J. Phys. Chem. C 2011, 115, 2428–2432

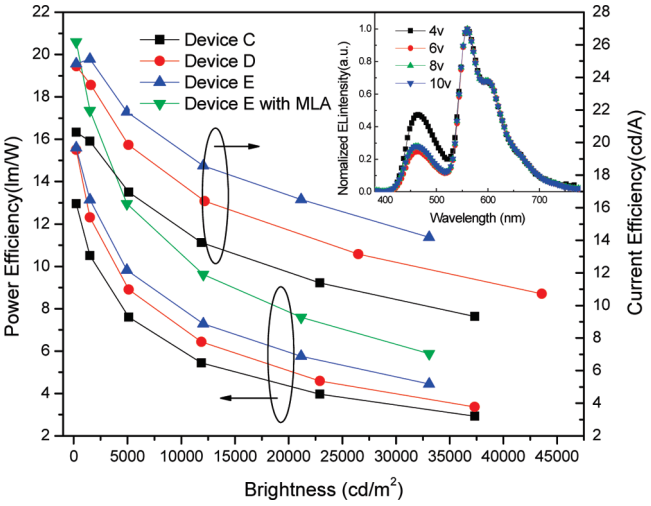

Figure 4. Brightness-efficiency characteristics of Devices C, D, and E and (inset) normalized EL spectra of Device E.

Table 1. Power Efficiency of Devices C−E at Different Brightness Levels

	1000 cd/m^2	3000 cd/m^2	5000 cd/m^2	10000 cd/m^2
Device C (lm/W)	11.5	9.3	7.7	6.0
Device D (lm/W)	13.7	10.9	9.0	7.2
Device E (lm/W)	14.1	11.7	9.8	8.0

$(BT)_2Ir(acac)$ (x nm)/DPV (25 − x nm)/Bphen (30 nm)/LiF/Al (x = 10, 12, and 14 nm for Device C, D, and E). Because more excitons will be generated in the CBP:$(BT)_2ir(acac)$ layer with the increasing thickness of the layer, the yellow emission from $(BT)_2ir(acac)$ increases reflecting the elevation of power and current efficiencies. The maximum power efficiency of Devices C−E are 12.9, 15.5, and 15.6 lm/W, respectively, and the maximum current efficiencies are 20.6, 24.7, and 24.8 cd/A, respectively (Figure 4). The power efficiency of Devices C−E at different brightness values are shown in Table 1. We obtained values of 24.8 cd/A, 15.6 lm/W, and 44910 cd/m^2 of a maximum current efficiency, power efficiency, and brightness for Device E. At a brightness of 1000 cd/m^2, the power efficiency of Device E can reach 14.1 lm/W. The power efficiency of Device E can reach about 10 lm/W at a very high brightness of 5000 cd/m^2. Considering the current efficiency roll-off from peak efficiency, Device E has 13.1% and 22.3% decreases in current efficiency at 5000 and 10000 cd/m^2, respectively. The inset in Figure 4 is the normalized EL spectra of device E at the voltage from 4 to 10 V. It can be clearly seen that the spectra remain fairly unchanged for 6, 8, and 10 V. When the bias voltage increases from 5 to 10 V, the CIE coordinates slightly change from (0.40, 0.42) to (0.38, 0.41). The efficiency roll-off of Device E is more significant than that of Device A. We think that it can be attributed to the TTA, which is more severe in Device E than in Device A. This is because that the concentration of the $(BT)_2Ir(acac)$ is higher and the phosphorescent emitting layer is thicker in Device E.

The EL efficiency of the device can be further increased by attaching a semispherical microlens array (MLA) outcoupling foil on glass substrate with an index-matched polymer. The diameter of the semisphere is about 60 μm, and the fill factor of the MLA is about 80% (see Figure 5). The brightness of the white device in the normal direction is increased; the calculated power efficiency of Device E, assuming a Lambertian emission, can reach 18.6 lm/W at 1000 cd/m^2 as shown in Figure 4. Besides, the CIE coordinates are only slightly shifted by (−0.006, 0.006).

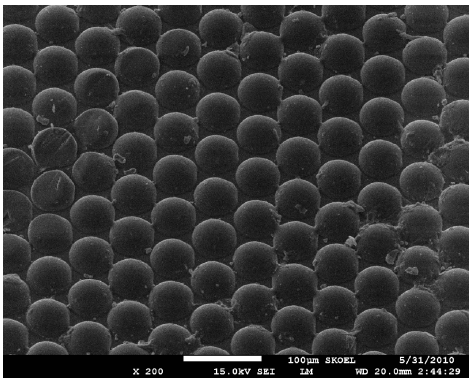

Figure 5. Scanning electron microscope image of the patterned microlens array.

In summary, we have demonstrated an efficient and color-stable fluorescent/phosphorescent hybrid WOLED. The fluorescent part is based on high hole and electron mobilities blue fluorophore DPV, of which carrier mobility is basically electric-field independent. The device has a normal direction power efficiency of 14.1 lm/W, which has a relatively slight efficiency roll-off and constant CIE coordinates. The power efficiency can be enhanced to 18.6 lm/W by attaching MLA outcoupling foil at 1000 cd/m^2. This result provides guidance in the fabrication of hybrid WOLEDs with optimum performance, such as power efficiency, efficiency roll-off, and color stability.

AUTHOR INFORMATION

Corresponding Author

*E-mail: xiewf@jlu.edu.cn (W. F. Xie); cchen@chem.sinica.edu.tw (C. T. Chen).

ACKNOWLEDGMENT

This work was supported by the National Nature Science Foundation of China (Grant Nos. 60937001, 60707016, 60723002, 11074096, 61077045). One of the authors (D.L.) acknowledges the State Key Laboratory on Integrated Optoelectronics, Jilin University, for financial support.

REFERENCES

(1) Tang, C. W.; VanSlyke, S. A. *Appl. Phys. Lett.* **1987**, *51*, 913.
(2) So, F.; Kido, J.; Burrows, P. *MRS Bull.* **2008**, *33*, 663.
(3) D'Andrade, B. W. *Nat. Photon.* **2007**, *1*, 33.
(4) Su, S. J.; Gonmori, E.; Sasabe, H.; Kido, J. *Adv. Mater.* **2008**, *20*, 4189.
(5) Chen, S. F.; Zhao, Z. Y.; Jie, Z. H.; Xie, W. F.; Zhao, Y.; Song, R. L.; Li, C. N.; Quan, B. F.; Liu, S. Y. *J. Phys. D: Appl. Phys.* **2006**, *39*, 3738.
(6) Xie, W. F.; Wu, Z. J.; Liu, S. Y.; Lee, S. T. *J. Phys. D: Appl. Phys.* **2003**, *36*, 2331.
(7) Xie, W. F.; Liu, S. Y.; Zhao, Y. *J. Phys. D: Appl. Phys.* **2003**, *36*, 1246.
(8) Chen, P.; Xie, W. F.; Li, J.; Guan, T.; Duan, Y.; Zhao, Y.; Liu, S. Y.; Ma, C. S. *Appl. Phys. Lett.* **2007**, *91*, 023505.
(9) Xu, Y. H.; Zhang, X. J.; Peng, J. B.; Niu, Q. L.; Cao, Y. *Semicond. Sci. Technol.* **2006**, *21*, 1373.

(10) D'Andrade, B. W.; Thompson, M. E.; Forrest, S. R. *Adv. Mater.* **2002,** *14*, 147.
(11) Guo, F. W.; Ma, D. G. *Appl. Phys. Lett.* **2005,** *87*, 173510.
(12) D'Andrade, B. W.; Holmes, R. J.; Forrest, S. R. *Adv. Mater.* **2004,** *16*, 624.
(13) Kalinowski, J.; Cocchi, M.; Virgili, D.; Fattori, V.; Williams, J. A. G. *Adv. Mater.* **2007,** *19*, 4000.
(14) Yang, H. S.; Zhao, Y.; Xie, W. F.; Shi, Y. W.; Hu, W.; Meng, Y. L.; Hou, J. Y.; Liu, S. Y. *Semicond. Sci. Technol.* **2006,** *21*, 1447.
(15) Guo, F. W.; Ma, D. G.; Wang, L. X.; Jing, X. B.; Wang, F. S. *Semicond. Sci. Technol.* **2005,** *20*, 310.
(16) Wang, Q.; Ding, J. Q.; Ma, D. G.; Cheng, Y. X.; Wang, L. X.; Jing, X. B.; Wang, F. S. *Adv. Funct. Mater.* **2009,** *19*, 84.
(17) Sun, Y. R.; Giebink, N. C.; Kanno, H.; Ma, B. W.; Thompson, M. E.; Forrest, S. R. *Nature* **2006,** *440*, 908.
(18) Ho, C. L.; Wong, W. Y.; Wang, Q.; Ma, D. G.; Wang, L. X.; Lin, Z. Y. *Adv. Funct. Mater.* **2008,** *18*, 928.
(19) Shih, P. I.; Shu, C. F.; Tung, Y. L.; Chi, Y. *Appl. Phys. Lett.* **2006,** *88*, 251110.
(20) Schwartz, G.; Pfeiffer, M.; Reineke, S.; Walzer, K.; Leo, K. *Adv. Mater.* **2007,** *19*, 3672.
(21) You, H.; Ma, D. G. *J. Phys. D: Appl. Phys.* **2008,** *41*, 155113.
(22) Wang, Q.; Ho, C. L.; Zhao, Y. B.; Ma, D. G.; Wong, W. Y.; Wang, L. X. *Org. Electron.* **2010,** *11*, 238.
(23) Zhang, T. Y.; Wang, J.; Li, T.; Liu, M.; Xie, W. F.; Liu, S. Y.; Liu, D. L.; Wu, C. L.; Chen, C. T. *J. Phys. Chem. C* **2010,** *114*, 4186–4189.
(24) Kim, S. H.; Jang, J.; Lee, J. Y. *Appl. Phys. Lett.* **2007,** *90*, 223505.
(25) Tse, S. C.; Kwok, K. C.; So, S. K. *Appl. Phys. Lett.* **2006,** *89*, 262102.
(26) Chi, C. C.; Chiang, C. L.; Liu, S. W.; Yueh, H.; Chen, C. T.; Chen, C. T. *J. Mater. Chem.* **2009,** *19*, 5561.
(27) Reineke, S.; Schwartz, G.; Walzer, K.; Falke, M.; Leo, K. *Appl. Phys. Lett.* **2009,** *94*, 163305.
(28) Lebental, M.; Choukri, H.; Chenais, S.; Foget, S.; Siove, A.; Geffoy, B.; Tutis, E. *Phys. Rev. B* **2009,** *79*, 165318.
(29) Baldo, M. A.; O'Brien, D. F.; Thompson, M. E.; Forrest, S. R. *Phys. Rev. B* **1999,** *60*, 14422.